Solution ^{1}H NMR Study of the Electronic Structure and Magnetic Properties of High-Spin Ferrous or Deoxy Myoglobins[⊥]

Catherine M. Bougault,[†,‡] Yi Dou,[§] Masao Ikeda-Saito,[§] Kevin C. Langry,[†] Kevin M. Smith,[†] and Gerd N. La Mar*[,†]

Contribution from the Department of Chemistry, University of California, Davis, California 95616, and Department of Physiology and Biophysics, School of Medicine, Case Western Reserve University, Cleveland, Ohio 44106-4970

Received September 11, 1997. Revised Manuscript Received December 15, 1997

Abstract: Solution 1D and 2D NMR, together with limited isotope labeling, have led to the assignment of the heme, axial His, and numerous heme contact residues in sperm whale, horse, and human deoxy myoglobin. The paramagnetic relaxivity leads to increased line widths and shorter T_1s with little compensation in increased dispersion due to dipolar shifts. Hence only limited, but crucial F helix standard backbone sequence specific assignment could be made for heme cavity residues. Numerous other residues with significant dipolar shifts could be assigned from the characteristic scalar connectivities and dipolar contacts to the heme predicted by the crystal structure. It is concluded that the complete and unambiguous assignment of the heme pyrrole substituent signals is not attainable by 2D NMR alone without either partial deuterium labeling of the heme or parallel assignment of key residues in dipolar contact with the heme; hence the present study revises some earlier assignments. The resulting dipolar shifts for nonligated residues, together with the crystal coordinates of deoxy myoglobin, were used to determine the orientation relative to the heme and the anisotropy of the paramagnetic susceptibility tensor. The significant anisotropy, $|\Delta\chi| \sim 1 \times 10^{-9}$ m^3/mol, however, is shown to result in dipolar shift with reciprocal square, rather than just reciprocal, absolute temperature dependence, which is indicative of large zero field splitting rather than *g*-tensor anisotropy. The appropriate equation for a $^5B_2$ ground state allows an estimate of the zero-field splitting, $D \sim -10$ cm^{-1}, which is in good agreement with earlier results. The present NMR data favor a spin-only magnetic moment with $S = 2$ and $D \sim -10$ cm^{-1} over a ground state with $S < 2$ and significant orbital contribution (Hendrich and Debrunner, 1989).

Introduction

Solution NMR studies of paramagnetic hemoglobin (Hb)[1] and myoglobin (Mb) derivatives have provided a wealth of unique information on the electronic, magnetic, and molecular properties of the active site that can be correlated with functional properties even if the particular oxidation/spin state does not have a direct physiological role (for reviews see ref 2). The dominant contact shifts for the ligated heme and axial His provide direct information on the orbital ground state and Fe-ligand binding,[3] while the necessarily dipolar shifts for nonligated residues yield information on the anisotropy and orientation of the paramagnetic susceptibility tensor, χ, in the molecular framework of the protein.[4,5] The most extensive and successful NMR studies have been carried out on the low-spin ferric, metMbCN and metHbCN complexes which exhibit both the most favorable hyperfine shift dispersion/relaxation ratio and the largest magnetic anisotropy. While the high-spin, ferric metMb, metHb exhibit a less favorable hyperfine shift dispersion to relaxation ratio, the origin of the hyperfine shifts has been established.[5,6] Unfortunately, the only functional paramagnetic state, high-spin ferrous or deoxy Mb, Hb, is the least understood,[7] not only from the point of NMR[8−11] but also with respect to its orbital ground state, Mössbauer[12−15] and EPR,[16] MCD[17] spectroscopy, and magnetic susceptibility data.[18]

* Address correspondence to Dr. Gerd N. La Mar, Department of Chemistry, University of California, Davis, Davis, CA 95616. Telephone: (916) 752-0958. FAX (916) 752-8995. e-mail: lamar@indigo.ucdavis.edu.

† University of California.

‡ Permanent address: Laboratoire LEDSS VI, UFR-CNRS 5616, Université Joseph Fourier BP 53, 38041 Grenoble, France.

§ Case Western Reserve University.

⊥ Keywords: heme pocket, dipolar shifts, deoxy myoglobin, paramagnetic anisotropy, NMR.

(1) Abbreviations used: NMR, nuclear magnetic resonance; Hb, hemoglobin; metHb, ferric hemoglobin; Mb, myoglobin; metMb, ferric myoglobin; metMbCN, cyanide ferric myoglobin; MbCO, carbonmonoxy myoglobin; DSS, sodium 2,2′-dimethyl-2-silapentane-5-sulfonate; MCD, magnetic circular dichroism; 1D, monodimensional; 2D, two-dimensional; NOE, nuclear Overhauser effect; NOESY, 2D nuclear Overhauser spectroscopy; TOCSY, total correlation spectroscopy; EPR, electron paramagnetic resonance; ZFS zero-field splitting.

(2) Ho, C.; Russu, I. M. *Adv. Enzymol.* **1981**, *76*, 275−292. Satterlee, J. D. *Ann. Rept. NMR Spectrosc.* **1986**, *17*, 79−178. Ho, C. *Adv. Protein Chem.* **1992**, *43*, 153−312. Bertini, I.; Turano, P.; Vila, A. J. *J. Chem. Rev.* **1993**, *93*, 2833−2932. Ho, C.; Perussi, J. R. *Methods Enzymol.* **1994**, *232*, 97−139.

(3) Shulman, R. G.; Glarum, S. H.; Karplus, M. *J. Mol. Biol.* **1971**, *57*, 93−115. Yamamoto, Y.; Inoue, Y.; Chûjô, R.; Suzuki, T. *Eur. J. Biochem.* **1990**, *189*, 567−573. Turner, D. L. *Eur. J. Biochem.* **1995**, *227*, 829−837.

(4) Rajarathnam, K.; La Mar, G. N.; Chiu, M. L.; Sligar, S. G. *J. Am. Chem. Soc.* **1992**, *114*, 9048−9058. Qin, J.; La Mar, G. N.; Cutruzzola, F.; Allocatelli, C. T.; Brancaccio, A.; Brunori, M. *Biophys. J.* **1993**, *65*, 2178−2190. Rajarathnam, K.; Qin, J.; La Mar, G. N.; Chiu, M. L.; Sligar, S. G. *Biochemistry* **1993**, *32*, 5670−5680. Wu, Y.; Basti, M.; Chiancone, E.; Ascoli, F.; La Mar, G. N. *Biochim. Biophys. Acta* **1996**, *1298*, 261−275.

(5) Kao, Y.-H.; Lecomte, J. T. J. *J. Am. Chem. Soc.* **1993**, *115*, 9754−9762.

(6) La Mar, G. N.; Budd, D. L.; Smith, K. M.; Langry, K. C. *J. Am. Chem. Soc.* **1980**, *102*, 1822−1827. Rajarathnam, K.; La Mar, G. N.; Chiu, M. L.; Sligar, S. G.; Singh, J. P.; Smith, K. M. *J. Am. Chem. Soc.* **1991**, *113*, 7886−7892.

(7) Hendrich, M. P.; Debrunner, P. G. *Biophys. J.* **1989**, *56*, 489−506.

(8) Yamamoto, Y.; Iwafune, K.; Chûjô, R.; Inoue, Y.; Imai, K.; Suzuki, T. *J. Biochem.* **1992**, *112*, 414−420.

S0002-7863(97)03197-1 CCC: $15.00
Published on Web 02/14/1998

The ^{1}H NMR spectra of high-spin ferrous hemoproteins are somewhat of a paradox. The very large hyperfine shifts for the axial His F8 are dominated by the contact interaction that reflects spin delocalization via Fe-imidazole σ bonding[19] and the ring labile $N_\delta H$ has served as a sensitive indicator of axial perturbations and a valuable empirical marker of deoxy Hb quaternary states and oxygen tension in muscle.[20] The hyperfine shifts for the heme, on the other hand, are relatively small, and it is likely that contact and dipolar contributions are similar in magnitude.[8−11,21] The heme shifts, nevertheless, have been shown to be sensitive to distal residue mutations and potentially provide information on how variable distal interactions modulate the nature of Fe-porphyrin bonding, the orbital ground state, and the magnetic anisotropy of the iron.[22] Structural analysis, however, first demands definitive assignments of the hyperfine shifted resonances, assessment of the contact versus dipolar contribution to the shifts. The presence of magnetic anisotropy manifests itself directly in NMR spectra as a dipolar shift, δ_{dip}, which in the limiting case of only axial anisotropy, $\Delta\chi_{ax}$, is given by[23]

$$\delta_{dip}(\text{calc}) = (1/3)[\Delta\chi_{ax}(3\cos^2\theta' - 1)R^3]\Gamma(\alpha,\beta,\gamma) \quad (1)$$

where θ' is the polar angle in a pseudo-symmetry (X-ray), iron-centered coordinate system, R is the proton−iron distance, and $\Gamma(\alpha,\beta,\gamma)$ is the Euler rotation matrix that relates the pseudo-symmetry axes to the magnetic axes where χ is diagonal.

Definitive heme assignments have been provided only for sperm whale deoxy Mb, where a combination of selective ^{2}H labeling of the methyls[9] and ^{13}C labeling, followed by ^{13}C−^{1}H decoupling of the vinyl groups[24] located the individual methyl and vinyl H_α signals and identified the mean shifts for the vinyl H_βs for each vinyl. Several 1D, 2D NMR studies have provided additional assignments on both sperm whale and horse deoxy Mb using the results from isotope labeling as a starting point.[8,10] A recent 2D NMR study on horse deoxy Mb has proposed a set of complete assignments for the heme pyrrole substituents and several nonligated residues.[11] Interestingly, the latter study identified[11] a strongly low-field shifted signal attributed to $C_\gamma H_3$ of Ile107(G8), which, at $R_{Fe} \sim 8$ Å, implies a substantial $\Delta\chi_{ax} \geq 4.3 \times 10^{-9}$ m^3/mol; the assignment in horse deoxy Mb for one of the 4-vinyl H_βs also differed dramatically from that previously reported for sperm whale deoxy Mb.[24] Moreover, an earlier pH study on both sperm whale and horse deoxy Mb had shown[21] that the low-field hyperfine shifted resonances included only two methyl groups, which in the former protein have been established to arise from the heme 5-CH_3 and 3-CH_3. These discrepancies in assignments must be resolved and the similarities or differences in the electronic/magnetic properties of the heme clarified for the otherwise very similar wild-type sperm whale, horse, and human Mbs prior to embarking on similar studies on mutants for any of these Mbs.

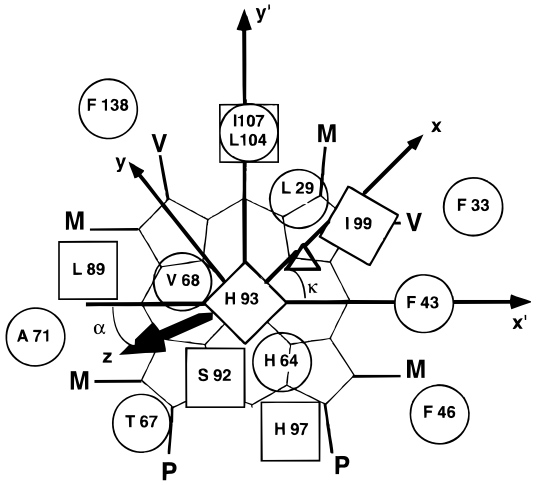

Figure 1. Schematic representation of the heme cavity of sperm whale deoxy Mb depicting the proximal (squares) and distal (circles) residues of interest, including a distal water molecule (triangle) hydrogen-bonded to His64(E7) and 3.8 Å from the iron; the heme substituents are labeled M (methyl), V (vinyl), and P (propionate). The pseudo-symmetry metal-centered X-ray coordinates, x', y', z' have the z' axis normal to the heme and the x' axis passing through the β, δ-meso positions. The magnetic axes (where χ is diagonal) are represented by x, y, z and are related to x', y', z' by $(x, y, z) = \Gamma(\alpha, \beta, \gamma)$ (x', y', z') where $\Gamma(\alpha, \beta, \gamma)$ are the Euler angles with β the tilt of the major magnetic axes, z, from the heme normal, z', (magnitude of tilt), and α is the angle made by the projection of z on the heme plane and the x' axis (direction of tilt); in the limit of axial anisotropy, γ is not relevant and is set to zero.

We present herein the results of a comprehensive NMR investigation of the heme cavity of deoxy Mb using a combination of 1D, 2D NMR and isotope labeling to definitively assign the heme, axial His, and other active site residues which exhibit dipolar shifts; target residues are shown in Figure 1. These latter shifts are used to determine the orientation of the magnetic axes, estimate the magnetic anisotropy, and separate the contact and dipolar contribution to the heme and axial His shift. We use standard sequence specific assignments[25] to identify the residues of interest to the extent allowed by the chemical shift dispersion and the line widths of backbone protons.

Experimental Section

Proteins. Sperm whale and horse metMb were purchased from Sigma Chemical Co. as lyophilized, salt-free powder and recombinant human Mb was prepared as described previously.[26] The samples were dissolved in 90% ^1H_2O: 10% ^2H_2O, 0.2 M in NaCl, and 50 mM

(9) La Mar, G. N.; Davis, N. L.; Johnson, R. D.; Smith, W. S.; Hauksson, J. B.; Budd, D. L.; Dalichow, F.; Langry, K. C.; Morris, I. K.; Smith, K. M. *J. Am. Chem. Soc.* **1993**, *115*, 3869−3876.
(10) Banci, L.; Bertini, I.; Marconi, S.; Pierattelli, R. *Eur. J. Biochem.* **1993**, *215*, 431−437.
(11) Busse, S. C.; Jue, T. *Biochemistry* **1994**, *33*, 10934−10943.
(12) Eicher, H.; Trautwein, A. *J. Chem. Phys.* **1969**, *50*, 2540−2551.
(13) Huynh B. H.; Papaefthymiou, G. C.; Yen, C. S.; Groves, J. L.; Wu, C. S. *J. Chem. Phys.* **1974**, *61*, 3750−3758.
(14) Eicher, H.; Bade, D.; Parak, F. *J. Chem. Phys.* **1976**, *64*, 1446−1455.
(15) (a) Kent, T. A.; Spartalian, K.; Lang, G. *J. Chem. Phys.* **1979**, *71*, 4899−4908. (b) Winkler, H.; Ding, X.-Q.; Burkardt, M.; Trautwein, A. X.; Parak, F. *Hyperfine Interactions* **1994**, *91*, 875−878.
(16) Hendrich, M. P.; Debrunner, P. G. *J. Magn. Reson.* **1987**, *78*, 133−141.
(17) Champion, P. M.; Sievers, A. J. *J. Chem. Phys.* **1980**, *72*, 1569−1582.
(18) Nakano, N.; Otsuka, J.; Tasaki, A. *Biochim. Biophys. Acta* **1971**, *236*, 222−233.
(19) Goff, H.; La Mar, G. N. *J. Am. Chem. Soc.* **1977**, *99*, 6599−6606. La Mar, G. N.; Budd, D. L.; Goff, H. *Biochem. Biophys. Res. Com.* **1977**, *77*, 104−110.
(20) Livingston, D. J.; La Mar, G. N.; Brown, W. D. *Science* **1983**, *220*, 71−73. Kreutzer, U.; Jue, T. *Eur. J. Biochem.* **1996**, *235*, 622−628.
(21) La Mar, G. N.; Budd, D. L.; Sick, H.; Gersonde, K. *Biochim. Biophys. Acta* **1978**, *537*, 270−283.
(22) La Mar, G. N.; Dalichow, F.; Zhao, X.; Dou, Y.; Ikeda-Saito, M.; Chiu, M. L.; Sligar, S. G. *J. Biol. Chem.* **1994**, *269*, 29629−29635.
(23) Jesson, J. P. In *NMR of Paramagnetic Molecules Principles and Applications*; La Mar, G. N., Horrocks, W. D., Jr., Holm, R. H., Eds.; Academic Press: New York, 1973; pp 2−51.
(24) Sankar, S. S.; La Mar, G. N.; Smith, K. M.; Fujinari, E. M. *Biochim. Biophys. Acta* **1987**, *912*, 220−229.
(25) Wüthrich, K. *NMR of Proteins and Nucleic Acids*; Wiley: New York, 1986.
(26) Ikeda-Saito, M.; Lutz, R. S.; Shelley, D. A.; McKelvey, E. J.; Mattera, R.; Hori, H. *J. Biol. Chem.* **1991**, *266*, 23641−23647.

phosphate buffer and converted to the metMbCN form by addition of 5 equiv of KCN; the cyanide excess was removed, and the samples were subsequently converted to 99% ^2H_2O solutions using an Amicon ultrafiltration cell. The sperm whale Mb sample reconstituted with hemin 90% deuterated at the vinyl β-positions is the same as that reported previously.[6] The 4−8 mM deoxy Mb solutions were prepared by first degassing the sample, followed by addition of 2 equiv of sodium dithionite (Nakarai Chemical, Tokyo). The solution pH was adjusted to ~8.5 by addition of degassed 0.2 M NaO^{2}H or ^{2}HCl; pH values were not corrected for the isotope effect.

NMR Data. NMR spectra were recorded at 500 MHz on a GE 500 spectrometer. Nonsaturating reference spectra and WEFT-spectra[27] (700 ms recycle time, 50−300 ms relaxation delay) to suppress the slowly relaxing diamagnetic envelope were recorded at 10−45 °C over 20 kHz (^2H_2O) and 100 kHz (^1H_2O) bandwidths. Rapidly exchanging labile protons in the 10−20 ppm window were detected using a 1:1 pulse sequence.[28] T_1s and line width ($\Delta = (\pi T_2)^{-1}$), dominated by Curie relaxation,[29,30] for other signals were estimated from

$$T_{1i}/T_{1j} = T_{2i}/T_{2j} = R_i^6/R_j^6 \quad (2)$$

using $T_1 \sim 60$ ms[9,11] and $(\pi T_2)^{-1} = 200$ Hz for a heme methyl with $R = 6.1$ Å. Steady-state NOEs were recorded in both ^1H_2O and ^2H_2O as described in detail previously[31,32] with a 30 ms decoupler pulse to effect ~50% saturation of the desired peak. Solvent suppression was achieved by direct saturation during the relaxation delay. 2D NOESY[33] and clean-TOCSY[34] data were recorded under two alternate conditions. Optimal detection of strongly relaxed resonances used $\tau_m = 20$ ms for TOCSY and $\tau_m = 50$ ms for NOESY spectra in ^2H_2O over a 20 kHz window with a recycle time of 380 ms with 512 t_1 blocks of 192 scans and 2048 t_2 points. Sequence-specific assignments used $\tau_m = 100$ ms for NOESY and $\tau_m = 20$ or 50 ms for TOCSY over a 20 kHz window with a 1.1 s recycle time. Each of 512 t_1 blocks consisted of 128 series of 2048 t_2 points. 1D spectra were exponentially apodized to introduce 1−50 Hz line broadening. 2D data sets were processed on a Silicon Graphics Indigo work station using the Felix 2.3 software. Fast repetition rate experiments in ^2H_2O were processed using both 60°-shifted sine-bell-squared function over 128 $t_1 \times 512$ t_2 points to optimally detect cross peaks between strongly relaxed resonances and 45°-shifted sine-bell-squared function over 256 $t_1 \times 1024$ t_2 points to detect cross peaks between strongly and weakly relaxed protons. 2D data in ^1H_2O were apodized by 30°-shifted sine-bell-squared function over the collected $t_1 \times t_2$ points. All data were zero-filled to 2048 × 2048 points prior to Fourier transformation.

Magnetic Axes and Hyperfine Shifts Determination. The observed chemical shift, δ_{DSS}(obs) is referenced to sodium 2,2′-dimethyl-2-silapentane-5-sulfonate, DSS, and consists of three contributions, the diamagnetic shift, δ_{dia}(obs or calc), the dipolar shift, δ_{dip}(obs or calc), and for the iron-ligated heme and axial His93(F8) protons, the contact shift δ_{con}(obs or calc).

$$\delta_{DSS}(\text{obs/calc}) = \delta_{dia}(\text{obs/calc}) + \delta_{hf}(\text{obs/calc}) = \delta_{dia}(\text{obs/calc}) + \delta_{dip}(\text{obs/calc}) + \delta_{con}(\text{obs/calc}) \quad (3)$$

The sum of the latter two terms is also labeled hyperfine shift, δ_{hf}. δ_{dia} is obtained from assigned resonances in MbCO,[35] and, if not available, is calculated via

$$\delta_{dia}(\text{calc}) = \delta_{tetr} + \delta_{sec} + \delta_{rc} \quad (4)$$

where δ_{tetr}, δ_{sec}, δ_{rc} are the tetrapeptide, secondary structure, and total ring current contributions[36] using the two available alternate deoxy Mb crystal coordinates.[37,38] Except for the distal His64(E7) and Val68(E11) side chains (see below), δ_{dia}(MbCO) and δ_{dia}(calc) generally differed by less than 0.2 ppm.[39]

The geometric factor in eq 1 was generated for the pseudo-symmetry axes x', y', z' generated from the crystal coordinates, whose z' coincides with the axial His N_ϵ-Fe vector and the x', y' axes lie parallel to the β,δ-meso-H, α,γ-meso-H directions, respectively; hence δ_{dip}(calc) in eq 1 automatically incorporates the effects of domming of the heme and the out-of-plane iron displacement characteristic of deoxy Mb. The orientation of the magnetic axes, $R(\alpha,\beta,\gamma)$, and the magnetic anisotropy, were determined from a four-parameter least-square search by minimizing the error function

$$\frac{F}{n}(\Delta\chi_{ax},\alpha,\beta,\gamma) = \sum_{\text{input}}[\delta_{dip}(\text{obs}) - \delta_{dip}(\text{calc})]^2 \quad (5)$$

where

$$\delta_{dip}(\text{obs}) = \delta_{DSS}(\text{obs}) - \delta_{dia}(\text{obs or calc}) \quad (6)$$

using as input those protons on nonligated residues[40] for which the slopes in the Curie plots (δ_{DSS}(obs) vs T^{-1} or T^{-2}) were found consistent with the sign and magnitude of δ_{dip}(obs)[41] and the deoxy Mb crystal coordinates.[37−39] For simplicity, $\Delta\chi_{rh}$ was set to zero (see Discussion). The optimized α, β (in the limit of axial anisotropy, γ is not relevant and is set to zero) were determined over a wide range of $\Delta\chi$ ranging for large positive to negative values.

Results

The 500 MHz ^{1}H NMR spectra in ^2H_2O for the resolved resonances of human, horse, and sperm whale deoxy Mb at 35 °C under slow repetition conditions are illustrated in Figure 2 (A−C, respectively), and the effect of temperature on the resolution of the resonances for the sperm whale Mb spectra is illustrated in Figure 2 (parts C (35 °C) and D (45 °C), respectively). Comparison of the low-field region of the sperm whale deoxy Mb spectra at 35 °C in ^1H_2O collected with a 1:1 pulse sequence with (Figure 2E) and without (Figure 2F) solvent saturation reveals the presence of three rapidly exchanging labile protons (labeled a−c) in the low-field window for the hyperfine shifted resonances. In the following sections we pursue in detail assignments on sperm whale deoxy Mb for which there exist several unambiguous assignments based on isotope labeling.[9,24] The assignments are later extended to horse and human deoxy Mb by observation of similar TOCSY and/or NOESY cross peak patterns.

Sperm Whale Deoxy Mb. Heme Assignment. As a starting point for our assignments by 1D/2D NMR we take the resolved heme methyls (5-CH_3, 3-CH_3) assigned from earlier deuterium labeling,[9] the position of the two vinyl H_αs, and the

(27) Gupta, R. K. *J. Magn. Reson.* **1976**, *24*, 461−465.
(28) Plateau, P.; Gueron, M. *J. Am. Chem. Soc.* **1982**, *104*, 7310−7311.
(29) Gueron, M. *J. Magn. Reson.* **1975**, *19*, 58−66. Vega, A. J.; Fiat, D. *Mol. Phys.* **1976**, *31*, 347−355.
(30) Johnson, M. E.; Fung, L. W.-M.; Ho, C. *J. Am. Chem. Soc.* **1977**, *99*, 1245−1250.
(31) Thanabal, V.; de Ropp, J. S.; La Mar, G. N. *J. Am. Chem. Soc.* **1987**, *109*, 265−272.
(32) La Mar, G. N.; de Ropp, J. S. *Biol. Magn. Reson.* **1993**, *12*, 1−78.
(33) Jeener, J.; Meier, B. H.; Bachmann, P.; Ernst, R. R. *J. Chem. Phys.* **1979**, *71*, 4546−4553.
(34) Griesinger, C.; Otting, G.; Wüthrich, K.; Ernst, R. R. *J. Am. Chem. Soc.* **1988**, *110*, 7870−7872.
(35) Thériault, Y.; Pochapsky, T. C.; Dalvit, C.; Chiu, M. L.; Sligar, S. G.; Wright, P. E. *J. Biomol. NMR* **1994**, *4*, 491−504.
(36) Cross, K. J.; Wright, P. E. *J. Magn. Reson.* **1985**, *64*, 220−231. Wishart, D. S.; Sykes, B. D.; Richards, F. M. *J. Mol. Biol.* **1991**, *222*, 311−333 and references therein.
(37) Takano, T. *J. Mol. Biol.* **1977**, *110*, 569−584.
(38) Phillips, S. E.; Schoenborn, B. P. *Nature* **1981**, *292*, 81−82.
(39) Both δ_{dia}(MbCO) and δ_{dia}(calc) based on the two deoxy Mb crystal coordinates[37,38] were used with only minor effects on the Euler angles and anisotropy. For the Val68(E11), His64(E7), and His97(FG3), the δ_{dia}(calc) was used in each case because these side chains have somewhat different orientations in MbCO and deoxy Mb.
(40) This set of 24 protons is Leu32(B13) $C_\delta H_3$; Thr39(C4) $C_\alpha H$, $C_\beta H$, $C_\gamma H_3$; Phe43(CD1) $C_\delta Hs$, $C_\epsilon Hs$; Val68(E11) $C_\gamma H_3$; Leu72(E15) $C_\gamma H$, $C_\delta H_3$s; Ala90(F5) $C_\alpha H$, $C_\beta H_3$; Ala94(F9) $C_\beta H_3$; His97(FG3) $C_\alpha H$, $C_\beta Hs$; Tyr103(G4) $C_\delta Hs$, $C_\epsilon Hs$; Ile107(G8) $C_\beta H$, $C_\gamma H_3$; Phe138(H15) $C_\delta Hs$, $C_\epsilon Hs$, $C_\xi H$; Tyr146(H23) $C_\delta Hs$, $C_\epsilon Hs$.

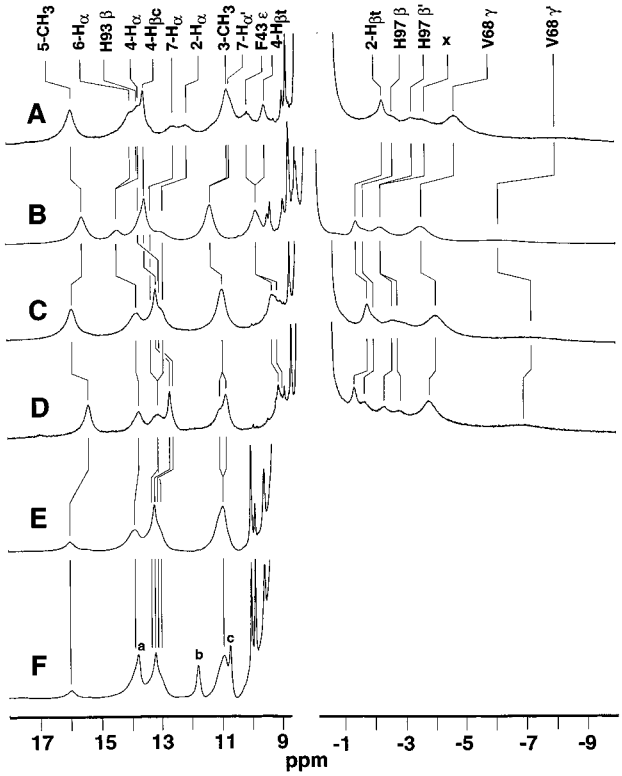

Figure 2. Resolved portion of the 500 MHz ^{1}H NMR spectra in ^2H_2O of: (**A**) human deoxy Mb at 35 °C; (**B**) horse deoxy Mb at 35 °C; and sperm whale deoxy Mb at (**C**) 35 °C and (**D**) 45 °C. The low-field resolved portion of the 500 MHz ^{1}H NMR spectra in ^1H_2O of sperm whale deoxy Mb in ^1H_2O, collected with a 1:1 pulse sequence with (**E**) and without (**F**) saturation of the ^1H_2O signal; rapidly exchanging labile proton signals are labeled a, b, c in (**F**). All solutions are 0.2 M in NaCl, 50 mM in phosphate and pH 8.4. The nonlabile protons are labeled in (**A**) and vertical lines show the position of these resonances in the remainder of the spectrum.

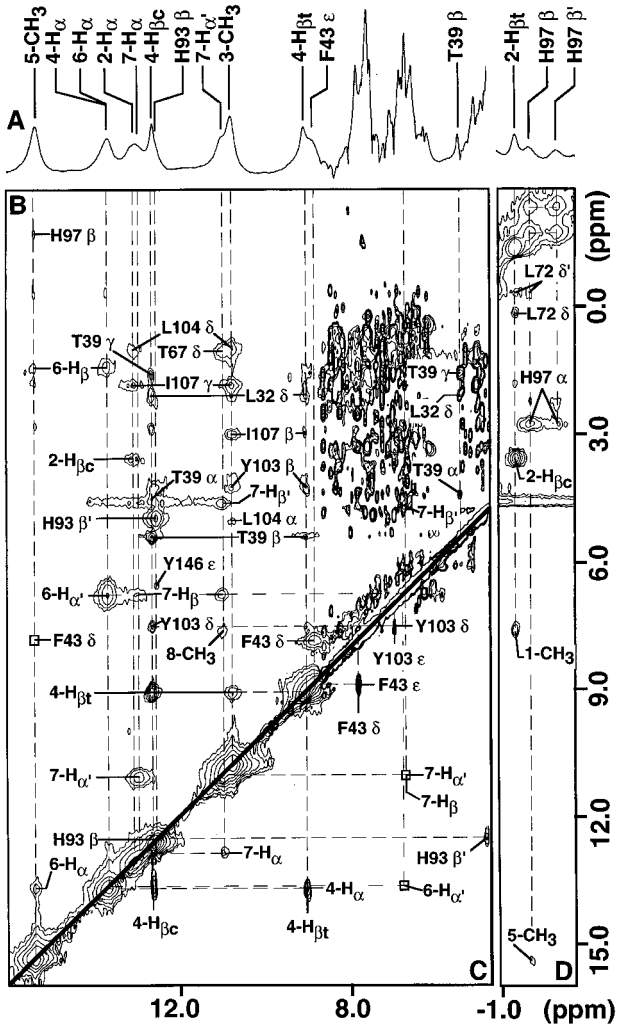

Figure 3. 500 MHz ^{1}H NMR spectra of sperm whale deoxy Mb in ^2H_2O 0.2 M NaCl, 50 mM phosphate at 45 °C: (**A**) reference WEFT spectrum (repetition rate 3 s^{-1}, delay 50 ms) for this resolved resonances; (**B**) and (**D**) portions of the NOESY spectrum (τ_m = 50 ms, repetition rate 2.6 s^{-1}), and (**C**) portion of TOCSY spectrum (mixing time 10 ms, repetition rate 2.6 s^{-1}). The peaks and cross peaks are labeled as assigned in the text; boxes show positions of cross peaks observed at lower contour levels.

mean chemical shifts for the vinyl H_βs obtained by ^{13}C decoupling of the ^{13}C labeled vinyl groups.[24] One of the vinyl H_α (13.69 ppm) exhibits two TOCSY cross peaks (Figure 3C) that locate the two H_βs (12.63, 9.06 ppm), and a NOESY cross peak from the 9.06 ppm peak to the 3-CH_3 (Figure 3B) identifies this spin system as the 4-vinyl group. The 2-vinyl H_α is expected to resonate in the composite peak at ~13 ppm. A weak TOCSY peak (not shown) and medium NOESY peak (Figure 3B) from 13.10 to 3.54 ppm, that locates one $2H_\beta$, and a strong NOESY cross peak from the latter $2H_\beta$ to the resolved $2H_\beta$ peak at −1.39 ppm (Figure 3D) identify the $2H_{\beta c}$ and $2H_{\beta t}$, respectively. The NOESY cross peak from $2H_{\beta t}$ to 7.60 ppm (Figure 3D) identifies the 1-CH_3, as expected from deuterium labeling.[9] The inability to detect the $2H_{\beta t}$-H_α TOCSY cross peak, previously reported[11] for horse deoxy Mb at 400 MHz, is likely due to the combination of insufficiently strong spin-lock field required by the larger shift dispersion (7.3 kHz) and the expected[30] increased line width at 500 MHz compared to that at 400 MHz.

A strongly relaxed single proton at 13.63 ppm, which exhibits a NOESY cross peak to 5-CH_3, yields strong NOESY (Figure 3B) and weak TOCSY (Figure 3C) cross peaks to its geminal partner (6.73 ppm) as well as a NOESY cross peak to a frequency common to the 5-CH_3 (1.38 ppm, Figure 3B); this pattern identifies the 6-propionate H_αs and one of its H_βs. A pair of partially resolved and strongly relaxed single protons exhibits the strong TOCSY (Figure 3C) and NOESY (Figure 3B) cross peak pattern characteristic for a CH_2 fragment, for which one proton (11.02 ppm) also exhibits a NOESY cross peak (Figure 3B) to 7.59 ppm where the 8-CH_3 is expected to resonate on the basis of deuterium labeling.[9] This locates the 7-propionate H_αs; the TOCSY/NOESY cross peaks to a less strongly relaxed and shifted methylene proton pair locate the 7-propionate H_βs. Since our assignment of the 4-vinyl $H_{\beta c}$ in sperm whale Mb differs significantly from that reported earlier[11] for horse deoxy Mb, we recorded a definitive NMR spectrum of sperm whale deoxy Mb reconstituted with heme perdeuterated at all vinyl β-positions which clearly shows that *both* 4-vinyl H_βs resonate in the low-field region, and one resolved 2-vinyl H_β appears in the upfield resolved region (not shown; see Supporting Information). The heme chemical shifts and their temperature dependence, represented by the slope and intercept at $T^{-1} = 0$ K in a Curie plot (shift *vs* reciprocal temperature), are listed in Table 1.

Axial His F8 Assignment. Our starting point is the assignment for the extremely low-field (Figure 4A) and strongly relaxed labile proton peak as that for the axial[19] His ring $N_\delta H$ (to be confirmed below by sequence specific assignments). Saturating the $N_\delta H$ in ^1H_2O resulted in a NOE to a nonlabile

Table 1. Heme and Axial His93(F8) ^{1}H NMR Chemical Shifts for Sperm Whale, Horse and Human Deoxy Mb in ^2H_2O, pH = 8.4 at 35 °C

	sperm whale deoxy Mb									
					$\Delta\chi = +0.96 \times 10^{-9}$ [e] (m^3/mol)		$\Delta\chi = -1.17 \times 10^{-9}$ [g] (m^3/mol)			
peak	δ_{DSS}(obs)[a] (ppm)	Curie slope[b] (ppm·K $\times 10^{-3}$)	$\delta_{int}(T^{-1})$[c] (ppm)	δ_{hf}(obs)[d] (ppm)	δ_{dip}(calc) (ppm)	δ_{con}(calc)[f] (ppm)	δ_{dip}(calc)	δ_{con}(calc)[h]	horse deoxy Mb δ_{DSS}(obs)[a] (ppm)	human deoxy Mb δ_{DSS}(obs)[a] (ppm)
1-CH_3	7.67	0.7	5	4.04	−3.12	7.16	−1.69	5.73	7.19	7.25
3-CH_3	10.91	1.1	7	7.12	2.27	4.95	1.77	5.35	10.97	10.73
5-CH_3	15.85	4.6	1	13.32	−2.36	15.7	−1.20	14.5	15.42	15.87
8-CH_3	7.71	1.2	4	4.12	0.62	3.50	2.14	1.98		
2-H_α	12.82	−2.7	22	4.39	−0.85	5.24	−2.64	7.03	12.66	12.06
2-$H_{\beta c}$	3.39	−1.5	8	−2.30	−2.80	0.50	−2.10	−0.20	3.39	3.15
2-$H_{\beta t}$	−1.84	−4.2	12	−7.57	−1.27	−6.30	−1.30	−6.27	−2.16	−2.35
4-H_α	13.81	11.7	10	5.19	0.62	4.57	3.22	1.97	13.41	13.62
4-$H_{\beta c}$	13.12	4.6	−2	6.83	1.37	5.46	2.16	4.67	13.25	13.48
4-$H_{\beta t}$	9.27	2.1	3	2.66	0.70	1.96	1.64	1.02	9.39	9.50
6-H_α	13.72	0.5	12	9.51	−1.64	7.87	−2.42	7.09	14.22	13.97
6-$H_{\alpha'}$	6.63	−1.3	11	2.42	−0.70	1.72	−2.90	−0.48	6.85	6.18
6-H_β	1.30	−0.8	4		1.26				1.58	1.65
7-H_α	13.21	2.7	4	9.00	2.09	6.91	0.40	8.60	13.25	12.53
7-$H_{\alpha'}$	10.97	−0.5	13	6.76	2.65	4.11	−0.13	6.89	10.97	10.58
7-H_β	6.96	2.1	∼0		1.25				6.80	6.49
7-$H_{\beta'}$	4.93	3.2	−6		1.95				4.35	4.52
H93(F8) N_pH[i]	8.80	0.4	8	1.10	0.19	0.9	0.97	0.1	8.80	9.00
H93(F8) $C_\beta H$	12.91	3.7	1	11.14	0.29	10.9	−2.19	13.3	13.38	13.76
H93(F8) $C_{\beta'}H$	5.07	1.2	1	3.30	0.92	2.4	−0.28	3.5	5.25	5.11
H93(F8) $C_\delta H$	42.2	8.8	14	41.1	1.93	39.2	−14.68	55.8	43.6	42.3
H93(F8) $C_\epsilon H$	42.2	8.8	14	40.6	14.7	25.8	39.85	0.7	43.6	42.3
H93(F8) $N_\delta H$[h]	75.2	17.6	18	65.8	0.37	65.4	3.10	62.3	76.1	77.6

[a] Chemical shift, in ppm, referenced to DSS via the residual solvent resonance. [b] Slope, in units of ppm·K, of the plot of δ_{DSS}(obs) versus reciprocal absolute temperature. [c] Intercept of the Curie plot at infinite temperature, in ppm. [d] Obtained from eq 3, using δ_{dia}(MbCO).[35,45] [e] Obtained from eq 1 for the magnetic axes with $\Delta\chi_{ax} = +0.96 \times 10^{-9}$ m^3/mol, $\alpha = 30°$, $\beta = 41°$, ($\gamma = 0°$) and the 1.4 Å deoxy Mb coordinates.[38] [f] Obtained from eq 3 using δ_{hf} in *d* and δ_{dip}(calc) in *e*. [g] Obtained from eq 1 for the magnetic axes with $\Delta\chi_{ax} = -1.17 \times 10^{-9}$ m^3/mol, $\alpha = 200°$, $\beta = 51°$, and the 1.4 Å crystal coordinates.[38] [h] Obtained from eq 3 using δ_{hf} in *d* and δ_{dip}(calc) in *g*. [i] Chemical shifts in ppm in ^1H_2O, pH = 8.4 at 35 °C.

and strongly relaxed single proton in the composite near 13 ppm (Figure 4B), which, in turn, exhibits both strong TOCSY (Figure 3C) and NOESY (Figure 3B) cross peaks in ^2H_2O to another broad, nonlabile proton at 4.95 ppm at 45 °C. These connectivities are unique to the geminal H_βs of His93(F8). A very strong NOE from the $N_\delta H$ to a labile proton at 8.80 ppm (Figure 4B), which also exhibits a moderate NOE in ^1H_2O (but not ^2H_2O) when the low-field His93(F8) H_β is saturated (Figure 4 (parts C and D, respectively)), uniquely locates the His93(F8) N_pH. The failure to detect additional TOCSY peaks to either the N_pH or the H_βs precludes the location of the $C_\alpha H$ of His 93(F8), likely because of the strong relaxation of both the H_βs (T_1 ∼40−70 ms, line width ∼175−300 Hz) and N_pH (line width ∼100 Hz; Figure 4B). These assignments, together with the two broad peaks observed near 42 ppm for the ring $C_\epsilon H$, $C_\delta H$ (again assigned on the basis of model compounds[9,19]), locate all but the $C_\alpha H$ for the axial His. The chemical shifts and slopes/intercepts in a Curie plot are included in Table 1.

Sequence-Specific Assignments. The assigned His93(F8) $N_\delta H$ and N_pH signals provide a route to locating portions of the F helix backbone. Saturating $N_\delta H$ yields two moderate intensity and three very weak NOEs to five labile protons (in addition to the His93(F8) N_pH) in the peptide proton window (Figure 5A), of which four participate in the sequential NH_i-NH_{i+1} NOESY cross peak pattern (Figure 5E) expected for a helix.[25] TOCSY reveals that NH_{i+1} in the four member series belongs to an Ala that experiences small but significant low-field shifts and moderate relaxation effects (weak cross peaks); the direction of the helix is established by the $C_\alpha H_{i+1}$-NH_{i+2} NOESY cross peaks. Saturating the His93(F8) $C_\beta H$ exhibits a moderate NOE to the $C_\alpha H$ of this Ala (Figure 4C), which uniquely identifies it as Ala 90(F5) via the expected $C_\alpha H_i$-$C_\beta H_{i+3}$ NOESY cross peaks for an α-helix. Most of the side chain protons for Leu89(F4), Gln91(F6), and Ser92(F7) were not located due to spectral congestion (and, in the case of Leu 89, expected extreme relaxation). The fifth N_pH NOE from His F8 $N_\delta H$ (Figure 5A) is the peptide NH of a TOCSY detected Ala spin-system (not shown) that gives a weak NOESY cross peak to His F8 N_pH (Figure 5E). This unambiguously assigns the later spin-system to Ala 94(F9). The N_pH_{92}-N_pH_{93} NOESY cross peak is not observed, likely because of the near degeneracy of the two shifts and adverse relaxation properties. The assignments of the two F helix Ala were confirmed by detecting the expected $C_\alpha H$ and $C_\beta H_3$ NOESY cross peaks to the Tyr146(H23) ring (see Figure 5 (parts C and D)). It is noteworthy that the present ^{1}H NMR data unambiguously and independently establish the His F8 $N_\delta H$ assignment of the extreme low-field signal in Figure 4A. Spectral congestion precluded the location of any other helical backbone fragment which could be connected to heme contacts (see Supporting Information for a schematic representation of the scalar and dipolar connectivity pattern in the F helix). On the other hand, a nearly complete A helix could be observed; these results are provided in Supporting Information. The chemical shift for assigned protons with significant dipolar shift, together with their intercepts in plots of shift versus T^{-1} and T^{-2}, are listed in Table 2; shifts for other assigned residues are listed in Supporting Information.

Assignments Based on the Crystal Structure. The heme and axial His assignments leave only six resolved or partially resolved signals, one on the low-field shoulder of the diamagnetic envelope and five upfield (two methyls and three single protons). Six nonligated residues in the heme pocket are expected to possess one or more protons that should exhibit stronger relaxation (T_1 < 50 ms) and larger line width (>100 Hz) than heme methyls using eq 2: Phe43(CD1), His64(E7),

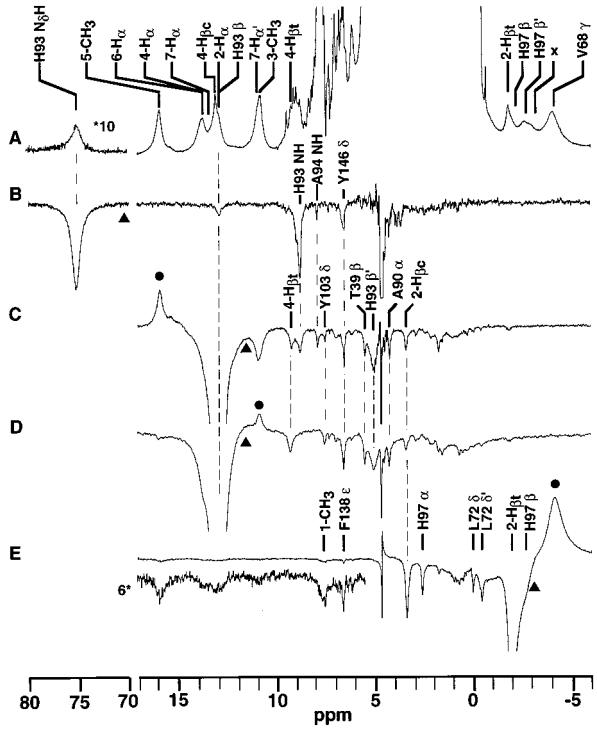

Figure 4. Resolved portion of the labeled 500 MHz ^{1}H NMR WEFT spectra (repetition rate 1.4 s^{-1}, relaxation delay 300 ms) of sperm whale deoxy Mb in (**A**) ^1H_2O, 0.2 M NaCl, pH 8.4 at 35 °C. Steady-state NOE difference spectra (irradiation time 50 ms) upon saturating: (**B**) His93(F8) $N_\delta H$ in ^1H_2O; (**C**) His93(F8) $C_\beta H$ (as well as partially saturating $2H_\alpha$, $4H_{\beta c}$ and $7H_\alpha$) in ^1H_2O, (**D**) His93(F8) $C_\beta H$ (as well as partially saturating 2-H_α, $4H_{\beta c}$ and $7H_\alpha$) in ^2H_2O, and (**E**) His97(FG3) $C_\beta H$ and $2H_{\beta t}$ in ^2H_2O. Relevant NOEs are labeled in each trace. The position of the reference frequency is shown by a triangle and the effect of off-resonance saturation is labeled by ●.

Val68(E11), Leu89(F4), His97(FG3), and Ile99(FG5). The predicted NOESY cross peak from 5-CH_3 to a resonance in the aromatic window (7.81 ppm) which exhibits NOESY (Figure 3B) and TOCSY (Figure 3C) cross peaks to the partially resolved low-field peak at 8.89 ppm, together with the Curie intercepts for both signals in the aromatic window, identify the Phe43(CD1) C_δHs, C_ϵHs peaks, respectively. The expected extreme relaxation ($T_1 \sim 12$ ms, line width > 500 Hz) for the $C_\zeta H$ precludes detection of the TOCSY/NOESY C_ϵHs-$C_\zeta H$ cross peak. A TOCSY/NOESY cross peak (see Figure 3D; TOCSY not shown) between two of the resolved upfield single proton signals at −1.72 and −2.34 ppm, together with a NOESY cross peak to 5-CH_3 (Figure 3B), identifies the C_βHs of His97(FG3); strong NOESY cross peaks from both H_βs to 2.73 ppm (Figure 3D) provide tentative assignment for the $C_\alpha H$.

The upfield resolved and strongly relaxed ($T_1 \sim 5$ ms) methyl peak (Figure 2 (parts C and D)) had been previously assigned[9,19] to the Val68(E7) $C_\gamma H_3$ on the basis of its unique proximity to the iron ($R \sim 4.8$ Å). A second, less strongly relaxed methyl peak at −3.86 ppm ($T_1 \sim 22$ ms, $R_{Fe} \sim 6.0$ Å) is consistent with arising from either Val68(E11) $C_\gamma H_3$ or Leu89(F4) $C_\delta H_3$. Saturation of this resonance yields a weak NOE to the broad 1-CH_3 peak (not shown), which is again consistent with either the Val or Leu methyl. However, the failure to detect a strong NOE to another less strongly relaxed methyl identifies it as Val68(E7) $C_\gamma H_3$. Prediction of extreme relaxation ($T_1 \leq 20$ ms, line width > 400 Hz) via eq 2 and artefacts introduced by the necessary rapid repetition rate[32] preclude detecting the needed NOESY cross peaks necessary to assign the His64(E7) $C_\epsilon H$, Leu89(F4) $C_\gamma H$, His97(FG3) $C_\delta H$, and Ile99(FG5) $C_\gamma H$ in ^2H_2O which, moreover, are expected (see below) to resonate within the diamagnetic envelope. The remaining partially resolved signal at −2.87 ppm (labeled X in Figure 2 (parts C and D)) with $T_1 \sim 30$ ms could arise from Val68(E11) $C_\alpha H$, Ile99(FG5) $C_\gamma H$, or Leu89(F4) $C_\gamma H$, but the absence of any TOCSY cross peak precludes differentiating between the possibilities.

Residues with only a moderately relaxed proton ($50 < T_1 < 120$ ms, 6 Å < R_{Fe} < 7 Å) as predicted by eq 2 include Thr67(E10), Phe138(H15) and the G helix residues Leu104(G5), Ile107(G8). Since only Thr67(E10) $C_\gamma H_3$ is close to the $7H_\alpha$, a NOESY cross peak (Figure 3B) to the methyl region locates $C_\gamma H_3$; spectral congestion precluded locating the remainder of the residue. Saturation of $2H_{\beta t}$ yields a NOE to the aromatic window (Figure 4E), which is part of a three-spin TOCSY (not shown; see Supporting Information) system and identifies the Phe138(H15) ring, where $C_\zeta H$ exhibits an upfield dipolar shift. NOESY cross peaks from an apparent methyl at 1.82 ppm to both 3-CH_3 and $2H_\alpha$ (Figure 3B) as well as a TOCSY cross peak from 1.82 ppm to an aliphatic proton at 2.98 ppm (not shown) that exhibits a NOESY cross peak to 3-CH_3 (Figure 3B) is diagnostic for the $C_\beta H$-$C_\gamma H_3$ fragment of Ile107(G8). The second methyl at 0.97 ppm which also exhibits NOESY cross peaks to both 3-CH_3, $2H_\alpha$ (Figure 3B) must arise from the $C_\delta H_3$ of Leu104(G5); a moderate NOESY cross peak from the 3-CH_3 to the $C_\alpha H$ spectral window identifies its $C_\alpha H$ at 5.04 ppm; TOCSY locates (not shown) two other protons, the likely C_βHs. The $C_\alpha H$, C_βHs of a TOCSY detected Phe exhibit NOESY cross peaks to the N_pH of our proposed Ile107(G8), as expected on an α-helical fragment,[25] and assigns it as Phe106(G7). The connectivities that provide the definitive assignments of Leu104(G5), Phe106(G7), and Ile108(G8) are provided in Supporting Information.

The remaining residues possess only weakly relaxed (R_{Fe} > 7 Å, T_1 > 150 ms) protons. A complete TOCSY-detected Thr (not shown; see Supporting Information) exhibits a NOESY cross peak to the 4-vinyl group (Figure 3B) and uniquely identifies Thr39(C4). A TOCSY detected isopropyl fragment (not shown) with both methyls exhibiting NOESY cross peaks to $2H_{\beta t}$ (Figure 3D) locates the terminus of Leu72(E15). The other expected weakly relaxed and weakly shifted Leu32(B13) $C_\delta H_3$ exhibits the expected NOESY peak to $4H_{\beta t}$, $4H_{\beta c}$ (Figure 3B), and Thr 39(C4) $C_\beta H$. Two two-spin aromatic side chains observed in the TOCSY map (not shown; see Supporting Information) exhibit NOEs to the His93(F8) C_βHs and $N_\delta H$ (Figure 4B−D) and 4-vinyl H_βs (Figure 3B) and uniquely identify Tyr146(H23) and Tyr103(G4), respectively. The chemical shifts for assigned protons with significant dipolar shift, together with their intercepts in plots of shift versus T^{-1} and T^{-2}, are listed in Table 2; other chemical shifts are listed in Supporting Information.

Low-Field Labile Protons. Three exchangeable proton signals located in the hyperfine shifted spectral window 10.5−15 ppm (Figure 2F) exhibit extensive, but incomplete, saturation upon irradiating the solvent signal (Figure 2E). Saturating the two peaks at 13.69 and 11.71 ppm led to the detection of two very strong peaks each in the aromatic spectral window diagnostic for two strongly hydrogen-bonded His side chains remote from the heme.[42] Very similar peaks with the same

(41) Emerson, S. D.; La Mar, G. N. *Biochemistry* **1990**, *29*, 1556−1566.

(42) While the chemical shifts for the labile proton signals in the hyperfine shifted region have obvious diamagnetic origin, steady-state NOEs and NOESY cross peaks involving these resonances, although exhibiting significant saturation transfer, must be carefully considered in analyzing either steady-state NOEs or NOESY cross peaks in the 10−15 ppm window.

Table 2. Chemical Shift of Dipolar Shifted Protons on Nonligated Heme Pocket Residues in Sperm Whale, Horse, and Human Deoxy Mbs[a]

		sperm whale Mb						horse Mb	human Mb
residue	proton	δ_{DSS}(obs)[b] (ppm)	δ_{dip}(obs)[c] (ppm)	T^{-1} slope[d] (ppm·K × 10^{-2})	$\delta_{int}(T^{-1})$[d] (ppm)	T^{-2} slope[e] (ppm·K^2 × 10^{-4})	$\delta_{int}(T^{-2})$[e] (ppm)	δ_{DSS}(obs)[b] (ppm)	δ_{DSS}(obs)[f] (ppm)
Leu32(B13)	$C_\delta H_3$	2.11	1.15	3.9	0.9	6.0	1.5	2.11	2.28
Thr39(C4)	$C_\alpha H$	4.49	0.30	3.7	3.3	5.7	3.9	4.43	4.52
	$C_\beta H$	5.48	0.68[g]	8.0	2.9	12.1	4.2	5.40	5.56
	$C_\gamma H_3$	1.54	0.40	5.8	−0.4	8.9	0.6	1.45	1.52
Phe43(CD1)	$C_\delta H$	7.82	0.53	1.9	7.2	2.8	7.5	7.97	8.29
	$C_\epsilon H$[f]	8.93	2.86	10.8	5.5	16.9	7.2	9.33	10.10
Thr67(E10)	$C\gamma H_3$[f]	1.11	−0.39	2.9	0.1	4.2	0.6	0.69[h]	0.40
Val68(E11)	$C_\gamma H_3$	−4.10	−3.51	−21.6	2.9	−30.6	−0.6	−4.60	−4.74
	$C_{\gamma'} H_3$	−7.36	−5.04	−20.6	−0.5	−29.2	−3.9	−7.59	−8.27
Leu72(E15)	$C_\gamma H$	0.50	−0.65	−5.7	2.4	−8.7	1.4	0.45	
	$C_\delta H_3$	0.01	−0.89	−4.4	1.4	−6.7	0.7	0.00	−0.02
	$C_{\delta'} H_3$	−0.43	−0.85	−5.6	1.4	−8.5	0.5	−0.49	
Ala90(F5)	$C_\alpha H$	4.22	0.78	4.8	2.7	7.3	3.4	4.33	
	$C_\beta H_3$	1.61	0.42	2.9	0.7	4.4	1.1	1.64	
Ala94(F9)	$C_\alpha H$	2.87	−0.24	1.2	2.5	1.8	2.7	2.74	
	$C_\beta H_3$	0.67	0.37	9.1	−2.3	14.0	−0.8	0.72	
His97(FG3)	$C_\alpha H$	2.59	−1.65	−13.7	7.1	−19.5	4.8	2.43	2.39
	$C_\beta H$	−2.11	−4.86	−35.3	9.4	−50.1	3.6	−2.49	−2.70
	$C_{\beta'} H$	−2.64	−4.29	−27.4	6.3	−39.0	1.8	−3.06	−3.27
Ile107(G8)	$C_\beta H$	3.00	0.84	2.0	2.4	2.8	2.7	2.86	2.82
	$C_\gamma H_3$	1.74	0.72	3.9	0.5	6.0	1.1	1.60	1.50
Phe138(H15)	$C_\delta H$	6.77	−0.32	−1.9	7.4	−2.8	7.1		
	$C_\epsilon H$	6.60	−0.54	−1.7	7.2	−2.6	6.9		
	$C_\zeta H$	6.16	−0.83	−9.7	9.2	−15.0	7.7		

[a] Chemical shifts for other heme pocket residues are listed in Supporting Information. [b] Chemical shifts in ppm, referenced to DSS via the solvent signal in ^1H_2O, 0.2 M NaCl, 50 mM phosphate, pH 8.4 at 35 °C, unless noted otherwise. [c] Obtained via eq 3 using δ_{dia}(MbCO)[35] at 35 °C, pH 5.6, unless noted otherwise. [d] Slopes and intercepts at $T \rightarrow \infty$ in plots of chemical shifts versus T^{-1}. [e] Slopes and intercepts at $T \rightarrow \infty$ in plots of chemical shifts versus T^{-2}. [f] In ^2H_2O, 0.2 M NaCl, 50 mM phosphate, pH 8.4 at 35 °C. [g] Obtained from eqs 3 and 4, where δ_{dia} is calculated using the ring current shifts in an α-helical fragment[36] and the 1.4 Å deoxy Mb crystal coordinates.[38] [h] Val 67(E10) $C_\gamma H_3$ chemical shift in horse deoxy Mb instead of the corresponding Thr residue in sperm whale and human Mb.

dipolar connectivity patterns have been observed and assigned in MbCO to His82(EF5) and His24(B5), respectively.[43] The third labile proton at 10.62 ppm is consistent with arising from Glu38(C6) N_pH, as reported for MbCO.[35]

Magnetic Axes Determination. The chemical shifts for assigned protons with significant dipolar shifts, together with their intercepts in plots of shift versus T^{-1} and T^{-2}, are listed in Table 2. The slope of the chemical shift in a plot of shift versus T^{-2} (Figure 6) or T^{-1} (Curie plot; not shown) for the assigned nonlabile protons with significant dipolar shifts (≥0.5 ppm) correlates reasonably well with δ_{dip}(obs) and indicates that the protons possess relatively fixed positions over the accessible temperature range.[41] Using the available data for these 24 signals,[40] a least-squared search for $\Gamma(\alpha, \beta, \gamma)$ was carried out as a function of $\Delta\chi_{ax}$, assuming that $\Delta\chi_{rh}$ is negligible. A plot of the residual error function, *F/n*, versus $\Delta\chi$ is shown in Figure 7. For $\Delta\chi < 0$, varying $\Delta\chi$ has only marginal effects on both α (200 ± 0°) and β (50 ± 10°), and the minimum in *F/n* occurs for $\Delta\chi = -1.17 \times 10^{-9}$ m^3/mol; γ is irrelevant for an axial system (not shown). In the case of $\Delta\chi > 0$, varying $\Delta\chi$ had stronger effects on the orientation of the tensor ($\alpha = 0 \pm 40°$, $\beta = 30 \pm 20°$), with the minimum in *F/n* occurring for $\Delta\chi = +0.96 \times 10^{-9}$ m^3/mol. Plots of the δ_{dip}(obs) (eq 6) versus δ_{dip}(calc) (via eq 3 and the optimum α, β), for the two minima are presented in Figure 8.

Predictions of δ_{dip}(calc) for significantly relaxed resonances which could not be assigned are considered next. The δ_{dip}(calc) and δ_{DSS}(calc), using eqs 1, 3, and 4 for the two minima, are listed in Table 3 where it is noted that dipolar shifts for the nonassigned, strongly relaxed resonances place the majority under the edges of the intense diamagnetic envelope where detection is severely hampered or under other less strongly relaxed resolved peaks. In each case, several resonances are predicted (Table 3) marginally outside the 0−10 ppm window, notably His64(E7) $N_\epsilon H$, $C_\epsilon H$, His97(FG3) $C_\delta H$ and the two Ile99(FG3) C_γHs for $\Delta\chi > 0$, and Phe43(CD1) $C_\zeta H$, His64(E7) $C_\epsilon H$, Ile99(FG5) C_γHs for $\Delta\chi < 0$ (Table 3). However, the expected extreme line width > 1 kHz and T_1s < 10 ms (via eq 2) for the His64(E7), His97(FG3) CHs and one Ile99(FG5) $C_\gamma H$ would render the peaks undetectable in the presence of narrower resonances in the same spectral window. The remaining unassigned peak X at −2.87 ppm at 45 °C (Figure 2A) likely arises from Ile99(FG5) $C_\gamma H$ and is better predicted for the positive than the negative anisotropy. A differentiation between the positive and negative anisotropy is not compelling, although the failure to observe the predicted Ile99(FG5) $C_\delta H_3$ (T_1 ~90 ms) at −6 ppm for negative $\Delta\chi_{ax}$ argues strongly for a positive sign for $\Delta\chi_{ax}$. Nevertheless, $|\Delta\chi|$ is well-bounded at ≤ 1 × 10^{-9} m^3/mol.

Assignment of Horse and Human Deoxy Mb. The comparison of the sperm whale and horse deoxy Mb spectra at the optimally resolved conditions at 35 °C (Figure 2 (parts C and B)) demonstrates that there is insufficient intensity for any resonance in the 12−14 ppm window to arise from a methyl, as discussed previously.[21] Detailed analyses of both the slow-repetition 2D NMR data in ^1H_2O as well as comparison of the steady-state NOE pattern upon saturating the 4-vinyl $H_{\beta c}$ located in the low-field composite at 13 ppm resulted in the same assignment for horse deoxy Mb as for sperm whale. The NOESY maps for horse and human deoxy Mb (not shown; see Supporting Information) convincingly demonstrate that the pattern of NOESY/TOCSY cross peaks observed for sperm whale deoxy Mb is conserved. The chemical shifts for the heme and axial His(F8) for both horse and human deoxy Mb are included in Table 1, and those for dipolar shifted protons on

(43) Yamamoto, Y. *J. Biochem.* **1996**, *120*, 126−132.

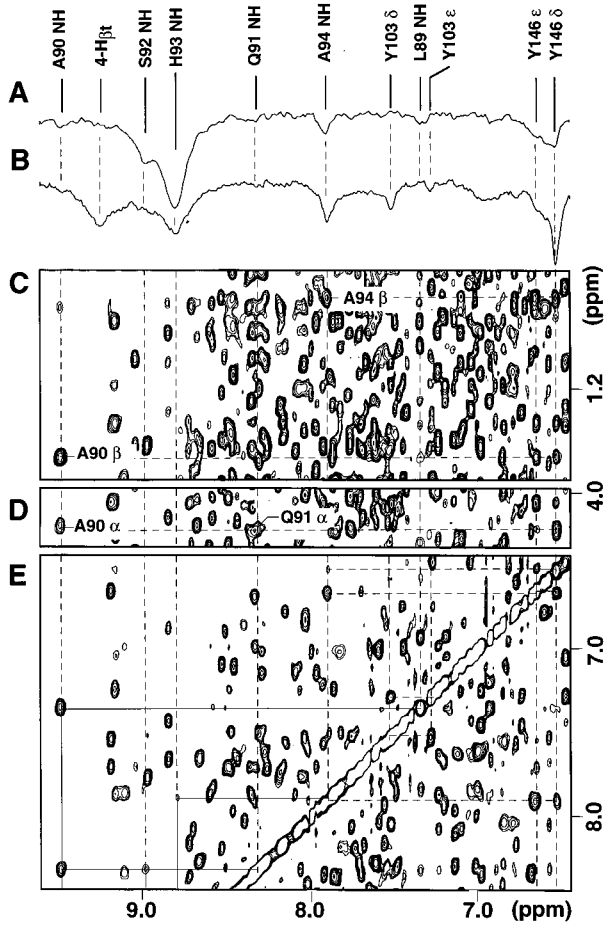

Figure 5. Steady-state NOEs in the aromatic spectral window for sperm whale deoxy Mb in ^1H_2O, 0.2 M NaCl, pH 8.4 at 35 °C upon saturating: (**A**) His93(F8) $N_\delta H$; (**B**) His93(F8) $C_\beta H$; (**C**−**E**) NOESY spectrum (irradiation time 100 ms, repetition rate 0.9 s^{-1}) for aromatic/peptide H spectral window showing the NH-NH (**E**), NH-$C_\alpha H$ (**D**), and NH-methyl (**C**) dipolar contacts of interest. Also shown in (**E**) are the two Tyr intra-ring cross peaks (all relevant TOCSY connectivities shown in Supporting Information). Solid lines mark inter-residue connectivities in the sequence-specific assignments and dotted lines mark intra-residue connectivities.

nonligated residues are included in Table 2 (others are listed in Supporting Information).

Discussion

Resonance Assignment. The heme pyrrole substituents in sperm whale deoxy Mb have all been identified in a manner that results in complete consistency with earlier isotope labeling.[9,24] Not detected are the four meso-Hs for which T_1 < 10 ms and line width > 500 Hz are expected, and which likely resonate under the diamagnetic window, as found earlier in model compounds.[19,44] With the available complete assignment, however, an analysis of the detected NOESY/TOCSY cross peaks among resolved resonances outside the diamagnetic and between resonances outside and within the diamagnetic envelope leads to the conclusion that *such data are insufficient to determine the heme assignments by 2D NMR alone*. Recourse to either isotope labeling of the heme methyls or parallel assignment of key nonligated residue side chains (*i.e.*, Phe43(CD1) with its characteristic contact to 5-CH_3, Phe138(H15) with its diagnostic contact to the 2-H_βs) is necessary. These latter

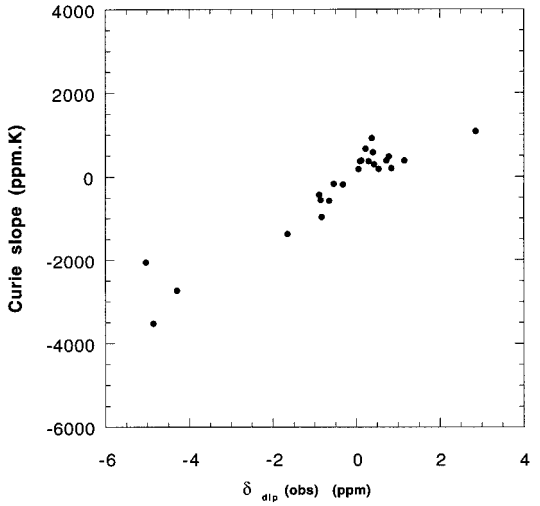

Figure 6. Plot of δ_{dip}(obs), obtained from eq 3 and δ_{dia}(MbCO), versus the slope of the plot of δ_{DSS}(obs) versus reciprocal absolute temperature squared for the 24 resonances used in the determination of the magnetic axes: Leu32(B13) $C_\delta H_3$; Thr39(C4) $C_\alpha H$, $C_\beta H$, $C_\gamma H_3$; Phe43(CD1) $C_\delta Hs$, $C_\epsilon Hs$; Val68(E11) $C_{\gamma'} H_3$; Leu72(E15) $C_\gamma H$, $C_\delta H_3$, $C_{\delta'} H_3$; Ala90(F5) $C_\alpha H$, $C_\beta H_3$; Ala94(F9) $C_\beta H_3$; His97(FG3) $C_\alpha H$, $C_\beta Hs$; Tyr103(G4) $C_\delta Hs$, $C_\epsilon Hs$; Ile107(G8) $C_\beta H$, $C_\gamma H_3$; Phe138(H15) $C_\delta Hs$, $C_\epsilon Hs$, $C_\zeta H$; Tyr146(H23) $C_\delta Hs$, $C_\epsilon Hs$.

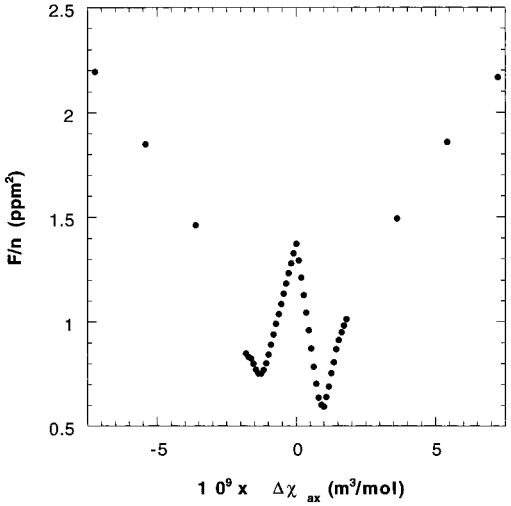

Figure 7. Plot of the residual error function, *F*/*n*, (via eqs 1−5) versus $\Delta\chi_{ax}$ ($\times 10^9$) in 10° increments of α, β ($\Delta\chi_{rh}$ is set to zero, and consequently $\gamma = 0$). The two local minima correspond, respectively, to $\Delta\chi_{ax} = -1.17 \times 10^{-9}$ m^3/mol and $\Delta\chi_{ax} = +0.96 \times 10^{-9}$ m^3/mol. The δ_{dia}(MbCO) shifts[35] and the 1.4 Å sperm whale deoxy Mb crystal structure[38] were used for the 24 input data in this calculation.

residues, in themselves, provide a challenge to assignment because the paramagnetism introduces a negligible dispersion to backbone HN-C_αHs over a diamagnetic derivative, while inducing significant relaxation for protons close to the iron. The result is that standard backbone assignments in deoxy Mb are considerably more limited than in either diamagnetic MbCO[45] or the paramagnetic metMbCN[46] complexes. The most problematic assignments involve the strongly relaxed but inconsequentially hyperfine shifted resonances which resonate close to or under the diamagnetic envelope 0−10 ppm. Both NOESY and TOCSY cross peak detection between two protons within the envelope is severely compromised not only by the strong

(44) Walker, F. A.; Simonis, U. *Biol. Magn. Reson.* **1993**, *12*, 133−274.

(45) Mabbutt, B. C.; Wright, P. E. *Biochim. Biophys. Acta* **1985**, *832*, 175−185.

(46) Qin, J.; La Mar, G. N. *J. Biomol. NMR* **1992**, *2*, 597−618.

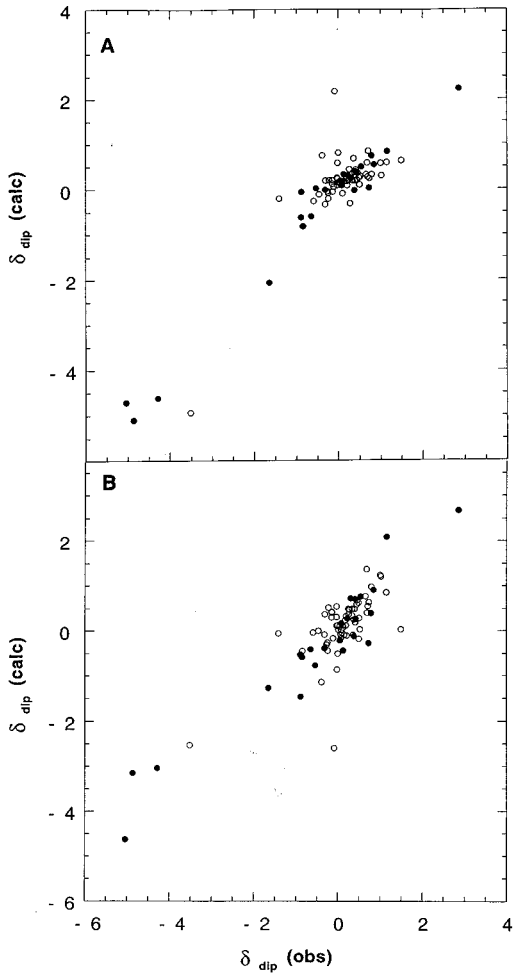

Figure 8. Plots of δ_{dip}(calc) (via eq 1) versus δ_{dip}(obs) for the optimized magnetic axes that give the local minima in the residual error function, *F/n* (eq 5) with (**A**) the positive absolute minimum in Figure 7 with $\Delta\chi_{ax} = +0.96 \times 10^{-9}$ m^3/mol, $\alpha = 30°$, $\beta = 41°$ ($\gamma = 0$) and residual $F/n = 0.12$ ppm^2, and (**B**) the negative local minimum in Figure 6 with $\Delta\chi_{ax} = -1.17 \times 10^{-9}$ m^3/mol, $\alpha = 200°$, $\beta = 51°$ ($\gamma = 0$) and residual $F/n = 0.35$ ppm^2. The data points corresponding to the resonances used to determine the magnetic axes are given in filled circles, and the other assigned protons are shown by open circles.

relaxation that decreases both NOESY (short T_1) and TOCSY (short T_2) but also the pulse repetition rate needed for effective sensitivity produces serious artefacts precisely in the same spectral window.[32]

In the case of horse deoxy Mb, the detected TOCSY and NOESY cross peak pattern as well as the individual shifts are essentially the same as those described in detail for sperm whale deoxy Mb. In human deoxy Mb, the 2D cross peak pattern is very similar to those of sperm whale and horse deoxy Mb, but with some minor systematic differences[47] in the dipolar contacts of Phe43(CD1).

Comparison with Previous Assignments. The present resonance positions of heme methyls, vinyl H_αs, and mean vinyl H_βs peaks are quantitatively consistent with earlier methyl deuteration and vinyl ^{13}C labeling in sperm whale deoxy Mb.[9,24] The propionate assignments are considered robust and are consistent with previous steady-state NOEs in sperm whale deoxy Mb based on the ^{2}H labeled heme methyl.[8] The His93(F8) $C_\beta H$ resonance at 13 ppm and the $N_\delta H$ at 75.6 ppm had also been proposed earlier[10] in sperm whale deoxy Mb, but the geminal partner $H_{\beta'}$ is shown here (by TOCSY peaks) to resonate at 5.6 ppm rather than the previously reported 11.4 ppm. The assignment of the upfield methyl to one Val68(E11) methyl on the basis of relaxation has been proposed previously.[8,9] The present steady-state NOE pattern provides additional support for the other Val $C_\gamma H_3$ at -3.86 ppm.

The extension of assignments for sperm whale to horse deoxy Mb provide several contradictions with previous reports.[8,11] Thus TOCSY clearly identifies a $4H_{\beta c}$ and His93(F8) H_β in this composite peak at ~13 ppm which were not recognized previously.[11] Moreover, the definitive assigned $6H_\alpha$, $4H_\alpha$, $7H_\alpha$ resonances account for *all of the remaining intensity of the 13 ppm composite*, obviating any possible additional low field methyl peaks. These results, moreover, are consistent with earlier ^{1}H NMR data[21] which excluded the presence of three low-field methyls in the complete pH titration of horse deoxy Mb. The present assignment of the His97(FG3) H_βs in sperm whale deoxy Mb agree with the earlier similar assignments in horse deoxy Mb.[11] The focal Ile104(G5) $C_\beta H$-$C_\gamma H_3$ fragment, proposed to resonate in the low-field window,[11] is clearly located in the diamagnetic envelope with only minimal hyperfine shift. The discrepancies between the present and previous horse deoxy Mb assignments emphasizes the problems in relying solely on 2D data for heme assignment without investigating in parallel the heme contact residues.

Magnetic Properties of the Iron(II). The observed dipolar shifts for nonligated residue protons in deoxy Mb are quantitatively accounted for by a moderate magnetic anisotropy $|\Delta\chi_{ax}|$ ~1×10^{-9} m^3/mol, about half that observed for low-spin iron(III) metMbCN, $\Delta\chi_{ax} = 2.2 \times 10^{-9}$ m^3/mol.[48] The magnetic anisotropy of deoxy Mb should be considered only an estimate since the tensor is unlikely to be axially symmetric (see below), as assumed in eq 1. However, the limited ^{1}H NMR data on dipolar shifts for definitively assigned protons, together with the uncertainty in the δ_{dip}(obs) for most resonances because of the small dipolar shifts for many protons and the uncertainties in δ_{dia}(obs or calc) preclude a meaningful five-parameter search for the three Euler angles and the two anisotropies $\Delta\chi_{ax}$, $\Delta\chi_{rh}$ with the available NMR data.

Previous consideration of the combined magnetic susceptibility,[18] Mössbauer[15] and EPR[7,16] data could not resolve two contrasting bases for the magnetic moment near the $S = 2$ spin-only value, a pure $S = 2$ ground state or a state (or states) with $S < 2$ and with significant orbital contribution to the magnetic moment. Significant orbital contributions to the magnetic moment in the low-symmetry ligand field of deoxy Mb would be expected to result in large *g*-tensor anisotropy as the source of the observed dipolar shift. Conversely, sizable dipolar shifts can arise from spin-only ions with $S > 1/2$ because of a large zero-field splitting (ZFS) constant *D*.[5,49−51] In fact, considering an orbitally nondegenerate, such as $^5B_2(d^2_{xy}d_{xz}d_{yz}d_{x^2-y^2}d_{z^2})$,

(47) The Phe43(CD1) $C_\delta H$-$5CH_3$ and Phe43(CD1) $C_\epsilon H$-Phe33(B14) ring cross peaks in human deoxy Mb are stronger and the Phe43(CD1) $C_\epsilon H$-$5CH_3$ cross peak is weaker than in sperm whale or horse Mb and indicates that Phe43(CD1) ring is placed slightly closer to the iron in human than in the other two deoxy Mbs. The closer placement of Phe43(CD1) to the iron in human than sperm whale deoxy Mb is consistent with the proposed closer placement of Val68(E11) to the iron.[9]

(48) Horrocks, W. D., Jr.; Greenberg, E. S. *Biochim. Biophys. Acta* **1973**, *322*, 38−44.

(49) Kurland, R. J.; McGarvey, B. R. *J. Magn. Reson.* **1970**, *2*, 286−301.

(50) Clark, K.; Dugad, L. B.; Bartsch, R. G.; Cusanovich, M. A.; La Mar, G. N. *J. Am. Chem. Soc.* **1996**, *118*, 4654−4664. de Ropp, J. S.; Mandal, P.; Brauer, S. L.; La Mar, G. N. *J. Am. Chem. Soc.* **1997**, *119*, 4732−4739.

(51) Champion, P. M.; Sivers, A. J. *J. Chem. Phys.* **1980**, *72*, 1569. Nakano, N.; Otsuka, J.; Tasaki, A. *Biochim. Biophys. Acta* **1972**, *236*, 222. Nakano, N.; Otsuka, J.; Tasaki, A. *Biochim. Biophys. Acta* **1972**, *278*, 355.

Table 3. Predicted Spectral Parameters for Unassigned Protons in the Heme Pocket of Sperm Whale Deoxy Mb at 35 °C

					fit with $\Delta\chi_{ax} = +0.96 \times 10^{-9}$ [c] (m^3/mol)		fit with $\Delta\chi_{ax} = -1.17 \times 10^{-9}$ [d] (m^3/mol)	
residue	proton	T_1[a] (ms)	line width[a] (kHz)	δ_{dia}(MbCO)[b] (ppm)	δ_{dip}(calc)[e] (ppm)	δ_{DSS}(calc)[f] (ppm)	δ_{dip}(calc)[e] (ppm)	δ_{DSS}(calc)[f] (ppm)
Phe43(CD1)	$C_\zeta H$	12	1.1	4.73	4.70	9.4	10.16	14.9
His64(E7)	$C_\delta H$	89	0.1	4.92	1.39	6.3	0.71	5.6
	$C_\epsilon H$	5	2.5	3.41[g]	7.37	10.8	−8.86	−5.5
	$N_\epsilon H$	4	3.0	3.88[g]	7.84	11.7	4.15	8.0
Val68(E11)	$C_\alpha H$	33	0.4	3.26	−4.61	−1.4	−3.61	−0.4
Leu89(F4)	$C_\gamma H$	21	0.6	0.58	3.12	3.7	6.44	7.0
	$C_{\delta'}H_3$	60	0.2	0.42	2.31	2.7	1.01	1.4
His97(FG3)	$C_\delta H$	11	1.2	2.34	−6.05	−3.7	−0.77	1.6
	$N_\epsilon H$	37	0.4	7.98[g]	−1.31	6.7	0.70	8.7
Ile99(FG5)	$C_\beta H$	68	0.2	1.40	−0.04	1.4	−2.65	−1.3
	$C_\gamma H$	43	0.3	0.20[g]	−3.78	−3.6	−5.42	−5.2
	$C_{\gamma'}H$	9	1.6	−0.55[g]	−3.05	−3.6	−3.15	−3.7
	$C_\gamma H_3$	74	0.2	1.13[g]	1.17	2.3	−1.12	0.0
	$C_\delta H_3$	90	0.2	1.21[g]	−1.47	−0.3	−0.71	−0.5
Ile107(G8)	$C_\delta H_3$	80	0.2	0.31	−0.50	−0.2	1.35	1.7

[a] Estimated using eq 2 with $T_1 = 57$ ms, line width = 200 Hz, and $R_{Fe} = 6.1$ Å for the heme 5-CH_3. [b] Taken from ref 35, unless noted otherwise. [c] Optimized magnetic axes with $\alpha = 30°$, $\beta = 41°$ ($\gamma = 0°$) using the 1.4 Å deoxy Mb crystal coordinates.[38] [d] Optimized magnetic axes with $\alpha = 200°$, $\beta = 51°$ ($\gamma = 0°$) using the 1.4 Å deoxy Mb crystal coordinates.[38] [e] Obtained via eq 1, and the α, β, values given in *c* or *d*. [f] Obtained from eqs 3 and 4 using the deoxy Mb crystal coordinates[38] and δ_{dip}(calc) from *e*. [g] Calculated via eq 4 and the deoxy Mb crystal coordinates.[38]

ground state proposed by Kent et al.[15a] for an axially-distorted Fe(II), the principal axes components of the susceptibility tensor, $\chi_{||}$ and $\chi_\perp$, can be related to the ZFS constant D and the g-tensor using the Van Vleck equation and the spin-Hamiltonian[49]

$$H = \beta_e g_{||} S_z H_z + \beta_e g_\perp [S_x H_x + S_y H_y] + D\left[S_z^2 - \frac{1}{3}S(S+1)\right] \quad (7)$$

$$\chi_{||} = \frac{2N_A \mu_0 g_{||}^2 \beta_e^2}{kT}\left[\frac{e^{-x} + 4e^{-4x}}{1 + 2e^{-x} + 2e^{-4x}}\right] \quad (8)$$

which yields

$$\chi_\perp = \frac{N_A \mu_0 g_\perp^2 \beta_e^2}{D}\left[\frac{6 - \frac{14}{3}e^{-x} - \frac{4}{3}e^{-4x}}{1 + 2e^{-x} + 2e^{-4x}}\right] \quad (9)$$

where $x = D/kT$, $g_{||}$ and $g_\perp$ are the principal axis components of the g-tensor in an axially distorted system. For the prevailing conditions ($D \ll kT$), this leads to

$$\Delta\chi_{ax} = \frac{N_A \mu_0 \beta_e^2}{kT}\left[2(g_{||}^2 - g_\perp^2) - \frac{14}{5}\frac{D}{kT}\left(g_{||}^2 + \frac{1}{2}g_\perp^2\right)\right] \quad (10)$$

Equation 10 reveals that dipolar shifts are expected to exhibit shifts $\propto T^{-1}$ behavior due to anisotropy of the g-tensor and T^{-2} behavior due to ZFS, as also predicted,[4] and observed for high-spin ferric hemoproteins.[5,50,51] Inspection of the intercepts at infinite temperature of the dipolar shift in T^{-1} and T^{-2} plots (Table 2) reveals *the latter, but not the former, are close to the expected* δ_{dia} and favor the dominant contribution to the magnetic anisotropy as originating in ZFS. For many protons $\delta_{int}(T^{-1})$ and $\delta_{int}(T^{-2})$ do not differ sufficiently to unambiguously establish the temperature dependence of the dipolar shifts because of the relatively small values of δ_{dip}(obs). However, the completely unacceptable $\delta_{int}(T^{-1})$ for the proton with sizable δ_{dip}(obs), *i.e.*, Phe43(CD1) C_ϵHs, His97(FG3) C_βHs and C_αH, clearly establish that only the T^{-2} behavior is an appropriate description for δ_{dip}(obs). Hence a ground state with $S < 2$ can be rejected.[7] The optimized $\Delta\chi_{ax} = 0.96 \times 10^{-9}$ m^3/mol and Euler angles from the NMR data, together with the deoxy Mb crystal structure,[37,38] yield $D \sim -10$ cm^{-1}, which is in excellent agreement in both sign and magnitude with previous estimates.[15b] It is noted that recent L-edge X-ray absorption spectroscopic data have been interpreted[52] on the basis of a well spaced ^5E orbital ground state, but the detailed analysis demanded lower than axial symmetry (*i.e.*, a term $E(S_x^2 - S_y^2)$ must be added to eq 7, with $E/D \sim 0.3$).

The two minima for $\Delta\chi_{ax}$ give rise to two perpendicular orientations of the unique axis. For the more likely positive $\Delta\chi_{ax}$, the major axis points in the general direction of the nonligated water molecular H-bonded to the distal His64(E7). There is no sound physical basis for expecting that this water should dominate over the axial His. On the one hand, it has been reported that the heme normal, in contrast to earlier studies,[14] is probably not a principal direction for the electric field gradient orientation.[15a] However, the restricted use of axial symmetry (due to data limitation to carry out meaningful five parameter searches), particularly in view of the significant rhombic asymmetry reflected in the L-edge X-ray absorption spectra,[52] make detailed interpretation of the orientation of the susceptibility imprudent at this time.

The very similar dipolar shifts for sperm whale and horse deoxy Mb, together with their nearly identical heme cavity structure, lead to the same $\Delta\chi$ for the two proteins. In the case of human deoxy Mb, it is noted that all δ_{dip}(obs) are *larger* (by ~10%; see Table 2) than for either horse or sperm whale deoxy Mb. Since all shifts change in a similar pattern, we conclude that the $\Delta\chi_{ax}$ in humans may be slightly larger than in the other two deoxy Mbs. The separation of the hyperfine shifts from the heme and axial His into dipolar and contact contribution, as shown in Table 1, reveals heme contact shifts which shed little new light on the iron−porphyrin bonding. It is likely that, as in the case of high-spin iron(III),[44] the observed contact shift reflects a combination of both σ and π spin delocalization, of which the former is likely dominant, as witnessed by large pyrrole-H and somewhat smaller pyrrole-methyl contact shifts.[9]

(52) Wang, H.; Peng, G.; Miller, L. M.; Scheuring, E. M.; George, S. J.; Chance, M. R.; Cramer, S. P. *J. Am. Chem. Soc.* **1997**, *119*, 4921−4928.

Acknowledgment. The authors are indebted to Dr. J. S. de Ropp of the UCD NMR Facility for experimental assistance and Dr. J.-M. Mouesca, CENG, Grenoble, for useful discussions. This research was supported by grants from the National Institutes of Health, HL 16087 (G.N.L.), HL 22252 (K.M.S.), and GM 51588 (M.I.-S.) and a fellowship to C.M.B. by the French Ministry of Foreign Affairs.

Supporting Information Available: Two tables (chemical shift of the assigned residues in the A helix; chemical shift for residue protons with negligible dipolar shifts) and seven figures (NOESY spectra for horse and human deoxy Mb; vinyl H_β identification by selective ^2H labeling in sperm whale deoxy Mb; TOCSY map for aromatic side chains and Thr39(C4) in sperm whale deoxy Mb; schematic representation of the scalar and dipolar connectivity patterns in part of the F and G helices; and NOESY and TOCSY maps for sequence specific assignments in the A helix) (11 pages). See any current masthead page for ordering and Web access instructions.

JA973197C